Received 12 December 2021; revised 11 January 2022; accepted 14 January 2022. Date of publication 18 January 2022; date of current version 22 February 2022.
The review of this article was arranged by Editor Z. Zhang.

Digital Object Identifier 10.1109/JEDS.2022.3144014

DFT Investigation on Targeted Gas Molecules Based on Zigzag GaN Nanoribbons for Nano Sensors

MANDAR JATKAR [1], KAMAL K. JHA [1] (Member, IEEE), AND SARAT K. PATRA [1,2] (Senior Member, IEEE)

1 Department of Electronics and Communication Engineering, Indian Institute of Information Technology Vadodara, Vadodara 382028, India
2 On Lien, National Institute of Technology Rourkela, Rourkela 769008, India

CORRESPONDING AUTHOR: M. JATKAR (e-mail: 201871002@iiitvadodara.ac.in)

This work was supported by the Indian Institute of Information Technology Vadodara (IIITV).

ABSTRACT In the present investigation, we studied the structural stability and electronic properties of bare and various adsorbed gas molecules ZGaNNR-2, ZGaNNR-4 and ZGaNNR-6 configurations. The electronic properties of all considered ZGaNNR configurations exhibit the metallic behaviour and it is verified through their band structures and densities of states. Based on binding energy/adsorption calculations, Bare-ZGaNNR-6 and O_2-ZGaNNR-6 configurations found the most thermostatic stable and energetically favoured configurations among all other considered ZGaNNRs. In transmission spectra, many distinct conductive states are observed in case of CO_2-ZGaNNR-6. The selectivity of CO_2/O_2 ZGaNNR has emerged as the most preferred (24.6) one among all considered configurations. CO_2-ZGaNNR-6 is emerged as the fast sensing device due to the lower recovery time (0.14 sec). The proposed device proves the high sensing capability towards the nano-scale devices.

INDEX TERMS Adsorption, sensing, selectivity, recovery time.

I. INTRODUCTION

With the tremendous growth in industrialization and commercial activities in recent years, severe air pollution has become a serious threat for all man-kinds [1], [2]. Increased amount of harmful pollutants such as CO_2 and CO is becoming a severe problem to human life [3]–[6]. The burning of fossil fuels is the primary sources of these greenhouse gases. As a result, monitoring and accurate identification of hazardous gases using effective sensors is the hot topic in the research fraternities [7]–[13]. Two-dimensional (2-D) devices have been used for the sensors applications by using different gas molecules [14]–[20]. Li *et al.* were investigated the WO_3 material theoretically for gas sensing applications [21]. The detecting the ethanol gas using mesoporous ZnO-Au composites has been investigated experimentally [22]. Martins *et al.* reviewed and addressed the some common 2-D sensors results using FETs [23]. 2-D materials like nanoribbons have been investigated for sensing applications due to their tunable properties [24], [25]. The electronic properties of the these materials are highly influenced by their width variations [26], [27] and edge structures [28]. Nanoribbons are suitable for different types applications including sensing devices [24], spitronics devices [29], nanoelectronics [30]–[32], VLSI interconnects [33] and piezoelectric devices [34]. Han *et al.* [35] and Pacile *et al.* [36] synthesized BN sheets using chemical-solution-derived methods and also using freely eliminated methods. Yogi *et al.* have investigated NO_2 and CO gas detection on zigzag and armchair nitride ribbons [37]–[39]. Sun *et al.* also investigated the gas molecules adsorption on defect-AlN ribbons [40]. Srivastava *et al.* studied on sensing PH_3 gas molecules [41]. Sachin *et al.* studied the stability of AlN monolayer and also investigated the group III-V elements, group IV compound using density functional theory (DFT) [42]. Tsipas *et al.* experimentally verified the stability of h-AlN using plasma method [43]. The vibrational, electronic and structural properties of pristine-AlN showed that the mono layer exhibits more stability with indirect band gaps and shows the direct band gaps for bulk compound [44], [45]. Gallium nitride nanoribbon (GaNNR) is little explored as a replacement

This work is licensed under a Creative Commons Attribution 4.0 License. For more information, see https://creativecommons.org/licenses/by/4.0/

of CMOS technology for future nanoelectronic devices due to its chemical stability, high thermal, high reverse breakdown voltage and wide band gap. GaN at bulk dimensions has already shown its potential of commercial viability for high power semiconductor devices [46], [47]. 2-D devices have been extensively used in sensors applications to detect ammonia, sulfur hexafluoride (SF_6), and acetone [48]–[50]. Owing to intrinsic wide band gap III-V nitrides play a vital role for designing the sensing devices, fast switches applications, RF signals electronic devices. On the other hand, it would be interesting to examine the band gap engineering of monolayer GaN to gauge its potential for replacing conventional sensor devices. However, there has been few research on gas sensors using GaNNR in the literature. We studied the gas molecules adsorption (CO_2, CO, NO and O_2) on ZGaNNRs using DFT method. Additionally, electronic properties, sensor properties and transport properties are also studied.

II. COMPUTATIONAL DETAIL

All the results presented here are investigated using a first-principles approach. ATK-VNL tool is used for calculating all parameters of adsorbed gas molecules on ZGaNNRs [51]. The ribbons are confined in X-Y directions and periodic with the Z direction. The investigations are conducted by using the super-cell approach with k-point of 1x1x50 sampling. We used 10Å vacuum space for eliminating interactions between ribbons and their periodic images. The cutoff energy of 70 Ry is chosen for each configuration and the optimization is conducted till the force on atoms are lower than 0.05 eV/Å. Generalized gradient approximations (GGA) - Perdew-Burke-Ernzerhof (PBE) calculation has been used for the correlation and exchange effects. The transition probability is calculated using the transmission spectra (TS). The following relation is used to estimate the $T(E_b,V_b)$ [29], [33].

$$T(E_b, V_b) = T_r\left[\tau_R(E_b, V_b)G^c(E_b, V_b)\tau_L(E_b, V_b)G^{c+}(E_b, V_b)\right] \tag{1}$$

where, $\tau_{R/L}$ is the coupling matrix of right/left electrodes and $G^{c/c+}(E_b, V_b)$ is the Green's function of the device region. T_r is the trace of the analogous matrix quantity. E_b is the transmission spectrum energy and V_b is finite bias.

III. STRUCTURAL PROPERTIES

To assess the gas molecules (CO_2, CO, NO and O_2) on ZGaNNR for sensing applications, we first analyzed the structure stability using binding energy (E_{BE}) per atom. Fig. 1 shows the optimized geometries of all considered gas molecules of ZGaNNR. All considered configurations are varied with a width (N_z) of 2, 4 and 6. N_z is used to define the ZGaNNR width, where N is the width and z represents the zigzag nanoribbon. Further, we studied Fermi energy (E_F) and binding energy (E_{BE}) of bare ZGaNNR-2, ZGaNNR-4 and ZGaNNR-6 configurations. The following relation is used to calculate the E_{BE} [38].

TABLE 1. Optimized bond length between two atoms of all considered (N_z = 6) configurations (All units are in Å).

Configurations	Ga-N	Ga-O	O-C	N-H	O-N	O-O
CO_2-ZGaNNR	1.81	1.85	1.35	1.01	-	-
CO-ZGaNNR	1.87	2.98	1.01	1.01	-	-
NO-ZGaNNR	1.82	1.91	-	1.01	1.25	-
O_2-ZGaNNR	1.82	1.85	-	1.01	-	1.33

TABLE 2. Width dependence of band gap (E_G), binding energy (E_{BE}) and Fermi energy (E_F) of bare ZGaNNR configurations.

Width (N_z)	E_G (eV)	E_{BE} (eV)	E_F (eV)
2	M	-5.34	-4.84
4	M	-5.83	-5.30
6	M	-6.03	-5.28

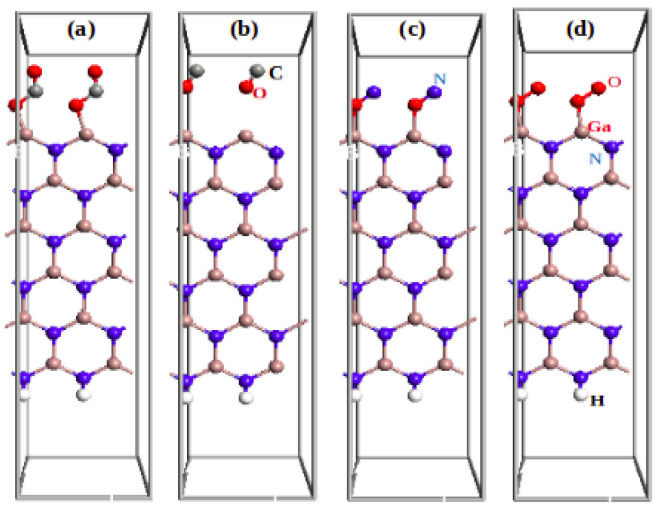

FIGURE 1. Schematic configurations of (a) CO_2-ZGaNNR-6, (b) CO-ZGaNNR-6, (c) NO-ZGaNNR-6 and (d) O_2-ZGaNNR-6.

$$E_{BE} = \frac{E_{Total} - mE_{Ga} - nE_N}{m+n} \tag{2}$$

where E_{Total}, $E_{Ga/N}$ indicate the total energies of bare ZGaNNRs and single isolated Ga/N atom. m, n are the total number atoms of Ga and N in ZGaNNRs, respectively. A higher negative value of E_{BE} are treated as the most stable configurations. Table 1 summarized the calculated optimized bond length between two atoms of all considered ($N_z = 6$) configurations. Table 2 compares the structural stability of bare ZGaNNR-2, ZGaNNR-4 and ZGaNNR-6, respectively. In the bare ZGaNNRs, ZGaNNR-6 is found as the most structural stable configuration, whereas bare-ZGaNNR-2 is the least stable preferred. The sequence of E_{BE} is noticed to be ZGaNNR-6> ZGaNNR-4>ZGaNNR-2, respectively. We also investigated the adsorption energy (E_{ADP}) of considered configurations using a relation of [41]

$$E_{ADP} = \frac{E_{Total} - E_{bare} - E_{CO_2/CO/NO/O_2}}{a+b} \tag{3}$$

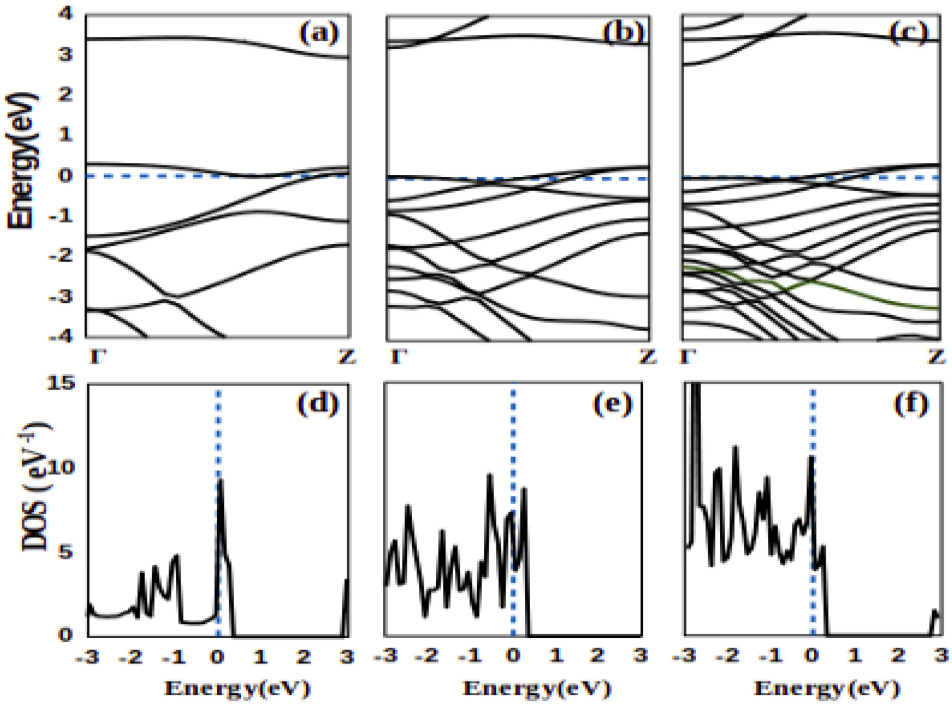

FIGURE 2. Band structures and DOS profiles of bare (a,d) ZGaNNR-2, (b,e) ZGaNNR-4 and (c,f) ZGaNNR-6.

TABLE 3. Width dependence of band gap (E_G), Fermi energy (E_F) and adsorption energy (E_{ADP}) of various gas ZGaNNR configurations.

Configurations	Width (N_z)	E_G (eV)	E_F (eV)	E_{ADP} (eV)
CO_2-ZGaNNR	2	M	-2.82	-1.62
	4	M	-2.91	-1.76
	6	M	-3.03	-1.77
CO-ZGaNNR	2	M	-3.99	-2.21
	4	M	-4.15	-2.40
	6	M	-4.33	-2.43
NO-ZGaNNR	2	M	-3.00	-2.66
	4	M	-3.13	-2.85
	6	0.05	-3.19	-2.86
O_2-ZGaNNR	2	M	-3.95	-3.03
	4	M	-3.96	-3.22
	6	M	-4.12	-3.24

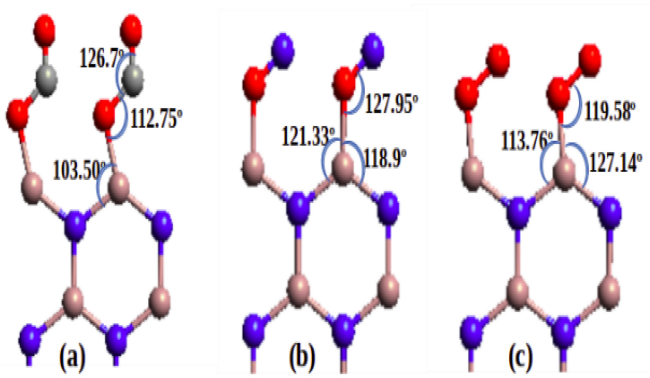

FIGURE 3. Schematics of bond angles of geometries after gas adsorption at upper edge for (a) CO_2-ZGaNNR-6, (b) NO-ZGaNNR-6 and (c) O_2-ZGaNNR-6.

where E_{Total}, E_{bare} and $E_{CO_2/CO/NO_2/NO/O_2}$ are the total energies of ZGaNNR configuration adsorption, bare ZGaNNR and isolated $CO_2/CO/NO_2/NO/O_2$ molecules and a, b are the total number of adsorbed molecules and H atoms present in the configuration. Table 3 compares the energetic feasibility of various gas molecules ZGaNNR-2, ZGaNNR-4 and ZGaNNR-6. It is noticed that the sequence of E_{ADP} is observed to be O_2-ZGaNNR> NO-ZGaNNR> CO-ZGaNNR> CO_2-ZGaNNR. The O_2-ZGaNNR configuration reported as most energetically favorable preceded by the NO-ZGaNNR configuration. Interestingly, it is noticed that as the ZGaNNR width increases with increased E_{ADP}. O_2-ZGaNNR-6 emerged as the most energetic feasible (−3.24eV) configuration, while CO_2-ZGaNNR-6 is the least energetic feasible (−1.77eV) configuration.

IV. ELECTRONIC PROPERTIES

Here, we have studied the electronic properties of the bare ZGaNNR-2, ZGaNNR-4 and ZGaNNR-6 and analyzed the width dependency. The width variation of E_F and E_G of bare ZGaNNRs are summarized in Table 2. All bare ZGaNNRs exhibit metallic in nature and it is verified through their band structure and densities of states (DOS). Fig. 2 depicts the band structures and DOS profiles of bare ZGaNNR-2, ZGaNNR-4 and ZGaNNR-6. Fig. 3 shows the schematics bond angle of optimized geometries after gas molecule adsorption. Here, we have noticed that, as bare ZGaNNR width increases with increased E_F. Bare-ZGaNNR-6 exhibits highest E_F as compared with bare-ZGaNNR-2 and bare-ZGaNNR-4 configurations. Further, the

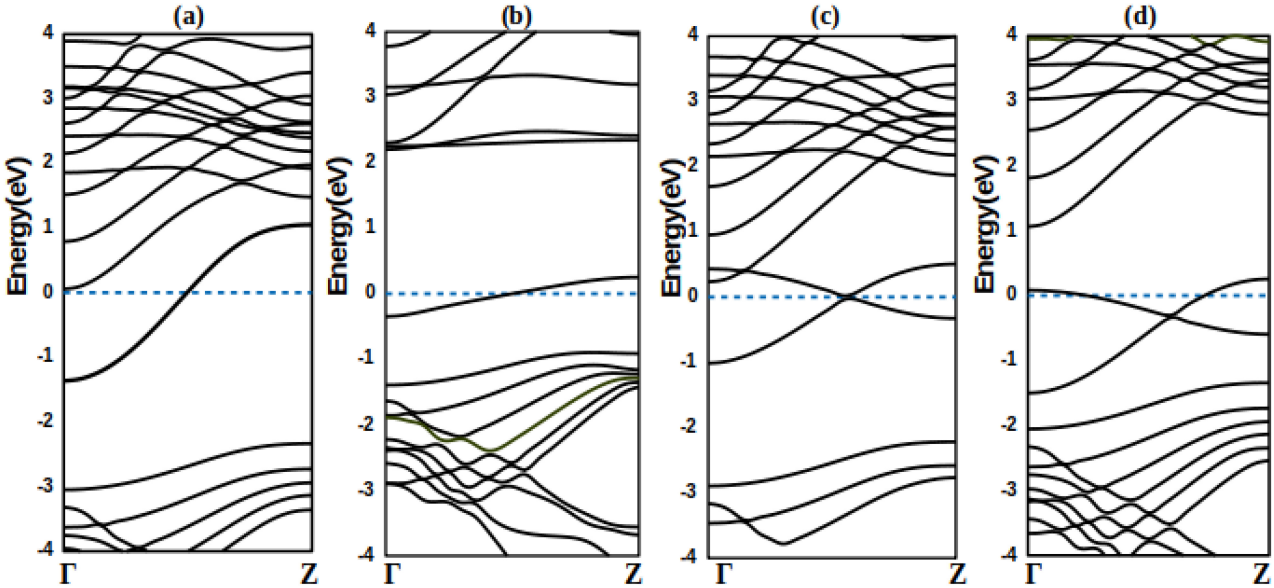

FIGURE 4. Band structures of considered configurations for (a) CO_2-ZGaNNR-6, (b) CO-ZGaNNR-6, (c) NO-ZGaNNR-6, and (d) O_2-ZGaNNR-6.

electronic properties of various gas molecules ZGaNNR are investigated with the help of DOS and band structures calculations. Here, we also investigated the width dependency of the CO_2, CO, NO and O_2 gas molecules ZGaNNR-2, ZGaNNR-4 and ZGaNNR-6 and analyzed the width dependence. The width variation of E_F and E_G of various gas molecules ZGaNNR are summarized in Table 3. CO_2, CO and O_2 gas molecules adsorbed on the ZGaNNR possess the metallic in nature and it is verified through their band structure and DOS profiles. Fig. 4(a,b,d) and Fig. 5(a,b,d) depicts the calculated band structures and DOS profiles of CO_2-ZGaNNR-6, CO-ZGaNNR-6, O_2-ZGaNNR-6. We observed semiconductor behavior in NO-ZGaNNR-6 configuration. Interestingly from Table 3, it is noticed that as the CO-ZGaNNR-6 width increases with increased E_F. CO-ZGaNNR-6 exhibits the highest E_F as compared to CO-ZGaNNR-4 and CO-ZGaNNR-2 configurations.

V. TRANSPORT PROPERTIES

To further verify the reported metallicity in various gas molecules ZGaNNRs, we used the two-probe model for calculating transmission spectra (TS) shown in Fig. 6. The two-probe model consists of a central region, right and left electrodes. Central scattering region is placed in between two electrodes. Fig. 7 depicts the calculated TS of various ZGaNNR-6 gas molecules for zero bias condition. The CO_2-ZGaNNR-6 have many distinct conductive states around the boundary orbitals shown in TS and also observed the peaks in TS at 0.2eV. The CO-ZGaNNR-6 contains multiple split edge states across the Fermi level. For this instant, the TS starts to lose its smoothness and Further, in NO-ZGaNNR-6, a scattering region blocks electrons from passing through the device. This leads to increased transmission peaks at the Fermi level and then decreases rapidly as the bias rises. In O_2-ZGaNNR-6, transmission peaks are almost low at 0 to 1eV. Further, at the negative bias of TS, a large block of transmissions originating at the bias window until they decrease to zero. This means that peaks increase before fading out, largely weakening around the Fermi level.

VI. SELECTIVITY

To investigate the sensing properties, we studied the selectivity (S) of ZGaNNRs for selected various gas molecules. The selectivity is the function of temperature. The Fig. 8 shows the S of CO, NO and O_2 gas molecules. The following relation is used to calculate the selectivity of X gas molecule with respect to Y gas molecule [37].

$$S_{X/Y} = \frac{A_X}{A_Y} e^{(-E_X+E_Y)/k_B T} \tag{4}$$

where A is the CO_2/CO/NO gas molecule interaction prefactor and O_2 gas molecule is equal to 10^{11} [37]. X and Y are the adsorption energies CO_2/CO/NO/O_2 gas molecules represented by E_{CO_2}, E_{CO}, E_{NO} and E_{O_2} respectively and T is the temperature in Kelvin and K_B is the Boltzmann constant. Temperature has a major role in various selectivity. The Fig. 8 shows the calculated selectivity of CO_2/CO, CO_2/NO, CO_2/O_2, CO/NO, CO/O_2 and NO/O_2 ZGaNNR-6 configurations. The NO gas molecule has a low selectivity for O_2 as compared with CO/NO selectivity. Further, studied the selectivity of ZGaNNRs for CO_2 gas molecules with respect to O_2, CO, NO gases. CO_2 has a high selectivity for O_2 followed by CO_2/NO selectivity. From Fig. 8, we have observed that selectivity of CO_2/O_2 on the ZGaNNR has emerged the most preferred (24.6) one amongst all considered configurations whereas selectivity of NO/O_2 is the least preferred (6.38) configuration.

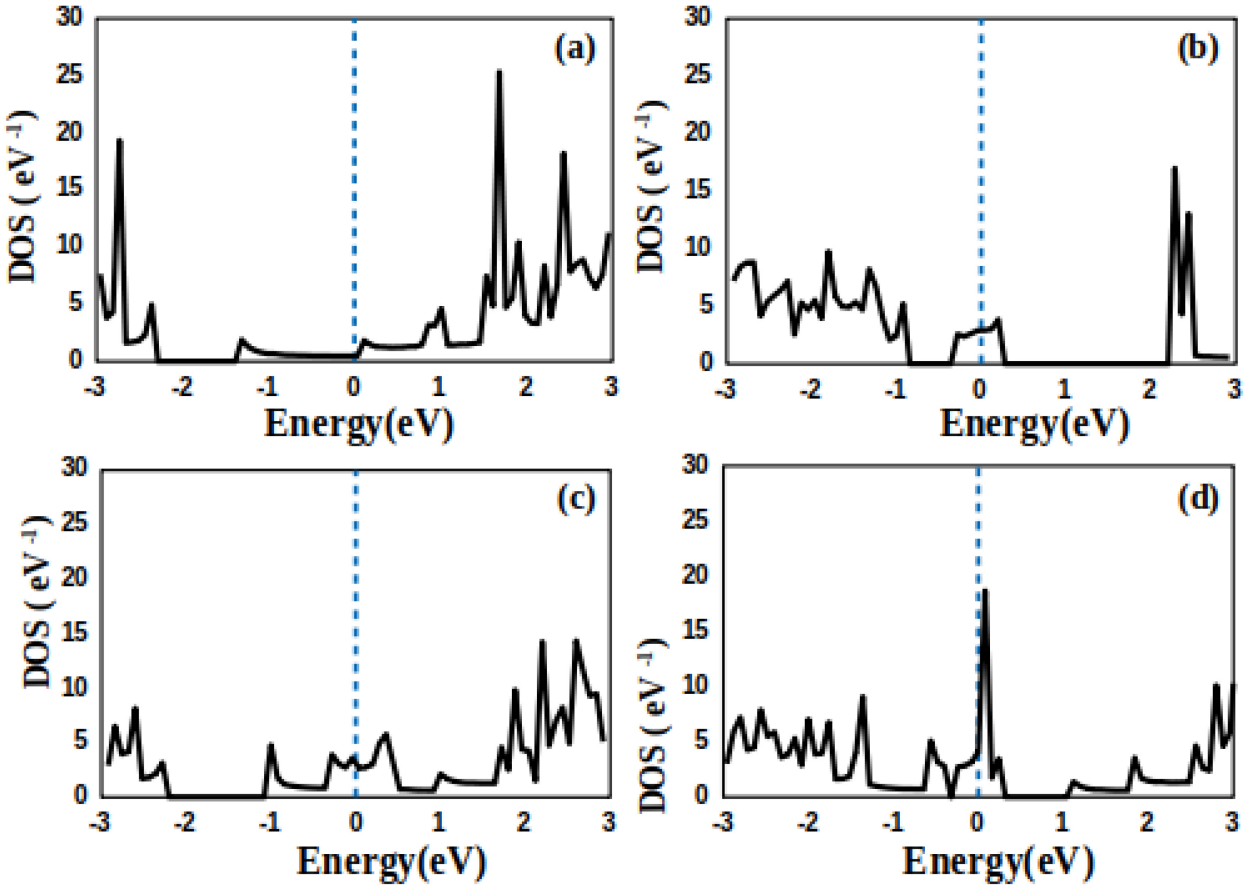

FIGURE 5. DOS profiles of considered configurations for (a) CO_2-ZGaNNR-6, (b) CO-ZGaNNR-6, (c) NO-ZGaNNR-6 and (d) O_2-ZGaNNR-6.

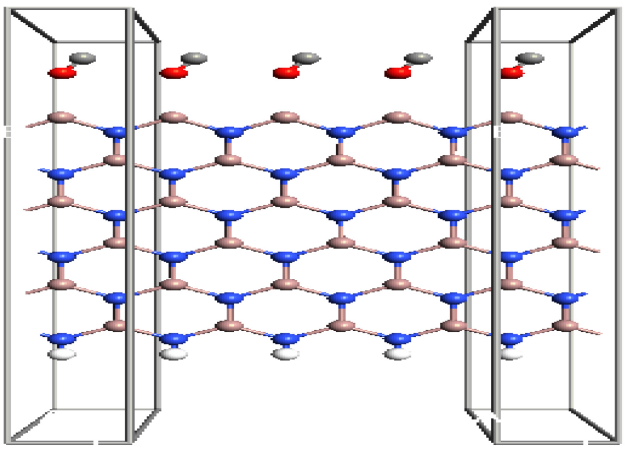

FIGURE 6. The standard two probe model of CO-ZGaNNR-6 and similar models are followed for other considered ZGaNNRs.

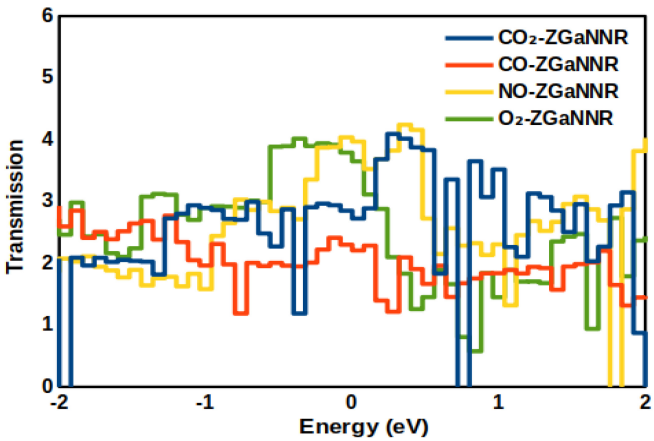

FIGURE 7. The transmission spectra of various ZGaNNR-6 configurations for zero bias condition.

VII. RECOVERY TIME

To investigate the recovery time (τ) of ZGaNNRs for various gas molecules, τ is mainly dependent on temperature. The calculated τ of various gas molecules of ZGaNNR as shown in Fig. 9. The following relation is used to estimate the τ on the various ZGaNNR gas molecules [37].

$$\tau = \upsilon^{-1} e^{(-E_{AD}/k_B T)} \tag{5}$$

where υ is the attempt frequency of bond breaking and the value is 10^{12} Hz [37]. E_{AD} is the adsorption energy of ZGaNNR-6 gas molecules. Temperature has a major role in recovery time as shown in Fig. 9. The T is inversely proportional to the recovery time. According to the τ study, it is clear that an increase in the temperature, τ also improves. The CO_2-ZGaNNR-6 configuration takes

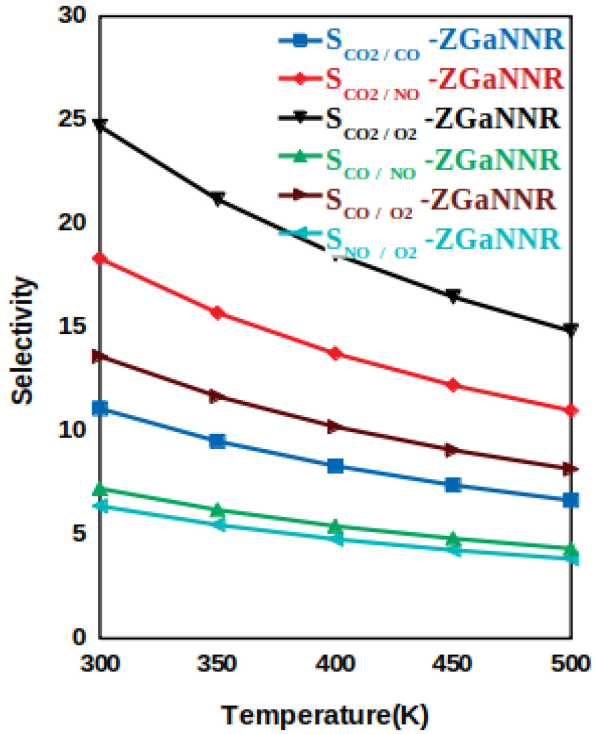

FIGURE 8. The calculated selectivity of CO_2/CO, CO_2/NO, CO_2/O_2, CO/NO, CO/O_2 and NO/O_2 ZGaNNR-6 configurations.

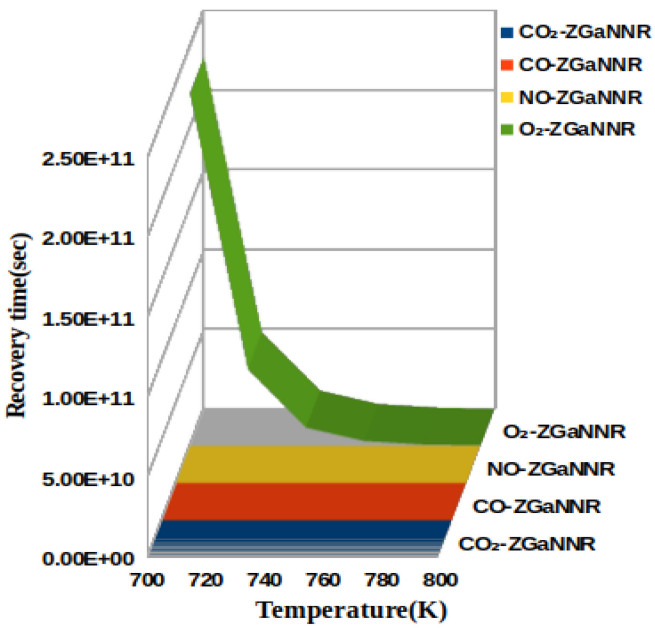

FIGURE 9. Recovery time calculations for various ZGaNNR-6 configurations.

approximately 5 sec to recover at 700K and gradually it decreases up to 0.14 sec at 800K. This states, the higher temperatures result in a faster τ, while lower temperatures result in a slower τ. Further, O_2-ZGaNNR-6 has a longer τ of 2.217×10^{11} sec at 700K. On the other hand, NO-ZGaNNR-6 configuration is expected to recover the time of 3.90×10^6 sec at 700K, further reduced to 1.04×10^6 sec for higher temperature. Due to the lower τ of CO_2-ZGaNNR-6 configuration is considered for fast sensing devices. The proposed device shows the potential for future high speed and low power nano-scale sensing devices.

VIII. CONCLUSION

In summary, DFT investigation shows that various gas molecules adsorption significantly effects the structural, electronic, transport and sensing properties of ZGaNNRs. Metallic behavior is observed in all considered ZGaNNR configurations. O_2-ZGaNNR-6 was found to be the most energetically favored(-3.24eV) configurations among various adsorbed gas molecules ZGaNNRs. The selectivity of CO_2/O_2 of ZGaNNR is the most preferred one (24.6) and also observed that, CO_2-ZGaNNR-6 is emerged as the fast sensing device due to the lower recovery time (0.14 sec). The proposed device shows the potential for futuristic robust nano-sensors.

ACKNOWLEDGMENT

The authors would like to thank PDPM-Indian Institute of Information Technology Design and Manufacturing Jabalpur for providing the computational facilities and Indian Institute of Information Technology Vadodara for infrastructural facilities.

REFERENCES

[1] B. Booth and N. Bellouin, "Black carbon and atmospheric feedbacks," *Nature*, vol. 519, no. 7542, pp. 167–168, 2015.

[2] A. Seaton, D. Godden, W. MacNee, and K. Donaldson, "Particulate air pollution and acute health effects," *Lancet*, vol. 345, no. 8943, pp. 176–178, 1995.

[3] J. M. Samet and M. J. Utell, "The risk of nitrogen dioxide: What have we learned from epidemiological and clinical studies?" *Toxicol. Ind. Health*, vol. 6, no. 2, pp. 247–262, 1990.

[4] D. M. Stieb *et al.*, "A national study of the association between traffic-related air pollution and adverse pregnancy outcomes in Canada, 1999–2008," *Environ. Res.*, vol. 148, pp. 513–526, Jul. 2016.

[5] I. Gregorczyk-Maga *et al.*, "Air pollution may affect the assessment of smoking habits by exhaled carbon monoxide measurements," *Environ. Res.*, vol. 172, pp. 258–265, May 2019.

[6] R. Beauchamp, J. S. Bus, J. A. Popp, C. J. Boreiko, L. Goldberg, and M. J. McKenna, "A critical review of the literature on carbon disulfide toxicity," *CRC Crit. Rev. Toxicol.*, vol. 11, no. 3, pp. 169–278, 1983.

[7] A. Afzal, N. Cioffi, L. Sabbatini, and L. Torsi, "NOx sensors based on semiconducting metal oxide nanostructures: Progress and perspectives," *Sens. Actuators B Chem.*, vols. 171–172, pp. 25–42, Aug./Sep. 2012.

[8] B. T. Marquis and J. F. Vetelino, "A semiconducting metal oxide sensor array for the detection of NOx and NH3," *Sens. Actuators B Chem.*, vol. 77, nos. 1–2, pp. 100–110, 2001.

[9] A. Fathalian, J. Jalilian, and S. Shahidi, "Effects of gas adsorption on the electronic properties of graphene nanoribbons," *Physica B Condens. Matter*, vol. 417, pp. 75–78, May 2013.

[10] R. Pearce, T. Iakimov, M. Andersson, L. Hultman, A. L. Spetz, and R. Yakimova, "Epitaxially grown graphene based gas sensors for ultra sensitive NO2 detection," *Sens. Actuators B Chem.*, vol. 155, no. 2, pp. 451–455, 2011.

[11] A. Sharma, M. Tomar, and V. Gupta, "Low temperature operating SnO2 thin film sensor loaded with WO3 micro-discs with enhanced response for NO2 gas," *Sens. Actuators B Chem.*, vol. 161, no. 1, pp. 1114–1118, 2012.
[12] C.-S. Huang, A. Murat, V. Babar, E. Montes, and U. Schwingenschlögl, "Adsorption of the gas molecules NH3, NO, NO2, and CO on borophene," *J. Phys. Chem. C*, vol. 122, no. 26, pp. 14665–14670, 2018.
[13] V. Babar, S. Sharma, and U. Schwingenschlögl, "Highly sensitive sensing of NO and NO2 gases by monolayer C3N," *Adv. Theory Simulat.*, vol. 1, no. 6, 2018, Art. no. 1700008.
[14] A. A. Peyghan, S. F. Rastegar, and N. L. Hadipour, "DFT study of NH3 adsorption on pristine, Ni-and Si-doped graphynes," *Phys. Lett. A*, vol. 378, nos. 30–31, pp. 2184–2190, 2014.
[15] H. J. Yoon, J. H. Yang, D. H. Jun, Z. Zhou, S. S. Yang, and M. M.-C. Cheng, "Carbon dioxide gas sensor using a graphene sheet," *Sens. Actuators B Chem.*, vol. 157, no. 1, pp. 310–313, 2011.
[16] M. Samadizadeh, A. A. Peyghan, and S. F. Rastegar, "Sensing behavior of BN nanosheet toward nitrous oxide: A DFT study," *Chin. Chem. Lett.*, vol. 26, no. 8, pp. 1042–1045, 2015.
[17] V. Nagarajan and R. Chandiramouli, "TeO2 nanostructures as a NO2 sensor: DFT investigation," *Comput. Theor. Chem.*, vol. 1049, pp. 20–27, Dec. 2014.
[18] B. Huang *et al.*, "Adsorption of gas molecules on graphene nanoribbons and its implication for nanoscale molecule sensor," *J. Phys. Chem. C*, vol. 112, no. 35, pp. 13442–13446, 2008.
[19] X.-L. Wei, Y.-P. Chen, W.-L. Liu, and J.-X. Zhong, "Enhanced gas sensor based on nitrogen-vacancy graphene nanoribbons," *Phys. Lett. A*, vol. 376, no. 4, pp. 559–562, 2012.
[20] M. M. Monshi, S. M. Aghaei, and I. Calizo, "Doping and defect-induced germanene: A superior media for sensing H2S, SO2, and CO2 gas molecules," *Surface Sci.*, vol. 665, pp. 96–102, Nov. 2017.
[21] J.-H. Li, J. Wu, and Y.-X. Yu, "DFT exploration of sensor performances of two-dimensional WO3 to ten small gases in terms of work function and band gap changes and IV responses," *Appl. Surface Sci.*, vol. 546, Apr. 2021, Art. no. 149104.
[22] Y. Kang, L. Zhang, W. Wang, and F. Yu, "Ethanol sensing properties and first principles study of Au supported on mesoporous ZnO derived from metal organic framework ZIF-8," *Sensors*, vol. 21, no. 13, p. 4352, 2021.
[23] E. de Freitas Martins, L. F. Pinotti, C. de Carvalho Castro Silva, and A. R. Rocha, "Addressing the theoretical and experimental aspects of low-dimensional-materials-based FET immunosensors: A review," *Chemosensors*, vol. 9, no. 7, p. 162, 2021.
[24] X.-J. Wu, M.-H. Wu, and X. C. Zeng, "Chemically decorated boron-nitride nanoribbons," *Front. Phys. China*, vol. 4, no. 3, pp. 367–372, 2009.
[25] H. M. Rai, N. K. Jaiswal, P. Srivastava, and R. Kurchania, "Electronic and transport properties of zigzag boron nitride nanoribbons," *J. Comput. Theor. Nanosci.*, vol. 10, no. 2, pp. 368–375, 2013.
[26] M. Y. Han, B. Özyilmaz, Y. Zhang, and P. Kim, "Energy band-gap engineering of graphene nanoribbons," *Phys. Rev. Lett.*, vol. 98, no. 20, 2007, Art. no. 206805.
[27] K. Nakada, M. Fujita, G. Dresselhaus, and M. S. Dresselhaus, "Edge state in graphene ribbons: Nanometer size effect and edge shape dependence," *Phys. Rev. B, Condens. Matter*, vol. 54, no. 24, 1996, Art. no. 17954.
[28] A. Du, S. C. Smith, and G. Lu, "First-principle studies of electronic structure and C-doping effect in boron nitride nanoribbon," *Chem. Phys. Lett.*, vol. 447, nos. 4–6, pp. 181–186, 2007.
[29] M. Jatkar, K. K. Jha, and S. K. Patra, "Fe-functionalized zigzag GaN nanoribbon for nanoscale spintronic-interconnect applications," *Appl. Phys. A, Solids Surface*, vol. 127, no. 6, p. 418, Jun. 2021.
[30] F. Zheng *et al.*, "Half metallicity along the edge of zigzag boron nitride nanoribbons," *Phys. Rev. B, Condens. Matter*, vol. 78, no. 20, 2008, Art. no. 205415.
[31] A. K. Nishad and R. Sharma, "Lithium-intercalated graphene interconnects: Prospects for on-chip applications," *IEEE J. Electron Devices Soc.*, vol. 4, no. 6, pp. 485–489, Nov. 2016.
[32] P. Xu and Z. Pan, "Collaborative applying the ultra-low-k dielectric and the high-k dielectric materials for performance enhancement in coupled multilayer graphene nanoribbon interconnects," *IEEE J. Electron Devices Soc.*, vol. 8, pp. 200–212, Feb. 2020.
[33] M. Jatkar, K. K. Jha, and S. K. Patra, "First-principles investigation of F-functionalized ZGNR-AGNR for nanoscale interconnect applications," *J. Comput. Electron.*, vol. 20, no. 4, pp. 1461–1470, 2021.
[34] J. Qi, X. Qian, L. Qi, J. Feng, D. Shi, and J. Li, "Strain-engineering of band gaps in piezoelectric boron nitride nanoribbons," *Nano Lett.*, vol. 12, no. 3, pp. 1224–1228, 2012.
[35] W.-Q. Han, L. Wu, Y. Zhu, K. Watanabe, and T. Taniguchi, "Structure of chemically derived mono-and few-atomic-layer boron nitride sheets," *Appl. Phys. Lett.*, vol. 93, no. 22, 2008, Art. no. 223103.
[36] D. Pacile, J. Meyer, Ç. Girit, and A. Zettl, "The two-dimensional phase of boron nitride: Few-atomic-layer sheets and suspended membranes," *Appl. Phys. Lett.*, vol. 92, no. 13, 2008, Art. no. 133107.
[37] R. Yogi and N. K. Jaiswal, "First-principle study of NO2 adsorption and detection on the edges of zigzag nitride nanoribbons," *Physica E Low-Dimensional Syst. Nanostruct.*, vol. 114, Oct. 2019, Art. no. 113575.
[38] R. Yogi and N. K. Jaiswal, "First principle insights of NO2 detection via III-V nitride nanoribbons with armchair edges," *Nano Exp.*, vol. 1, no. 1, 2020, Art. no. 010059.
[39] R. Yogi and N. K. Jaiswal, "Adsorption of CO gas molecules on zigzag BN/AlN nanoribbons for nano sensor applications," *Phys. Lett. A*, vol. 383, no. 6, pp. 532–538, 2019.
[40] G. Sun, P. Zhao, W. Zhang, H. Li, and C. He, "Adsorption of gas molecules on armchair AlN nanoribbons with a dangling bond defect by using density functional theory," *Mater. Chem. Phys.*, vol. 186, pp. 305–311, Jan. 2017.
[41] P. Srivastava, N. K. Jaiswal, and V. Sharma, "First-principles investigation of armchair boron nitride nanoribbons for sensing PH3 gas molecules," *Superlattices Microstruct.*, vol. 73, pp. 350–358, Sep. 2014.
[42] H. Şahin *et al.*, "Monolayer honeycomb structures of group-IV elements and III-V binary compounds: First-principles calculations," *Phys. Rev. B, Condens. Matter*, vol. 80, no. 15, 2009, Art. no. 155453.
[43] P. Tsipas *et al.*, "Evidence for graphite-like hexagonal AlN nanosheets epitaxially grown on single crystal Ag (111)," *Appl. Phys. Lett.*, vol. 103, no. 25, 2013, Art. no. 251605.
[44] C. Bacaksiz, H. Sahin, H. Ozaydin, S. Horzum, R. T. Senger, and F. M. Peeters, "Hexagonal AlN: Dimensional-crossover-driven band-gap transition," *Phys. Rev. B, Condens. Matter*, vol. 91, no. 8, 2015, Art. no. 085430.
[45] Y. Dai, X. Chen, and C. Jiang, "Electronic structures of zigzag AlN, GaN nanoribbons and AlxGa1- xN nanoribbon heterojunctions: First-principles study," *Physica B Condens. Matter*, vol. 407, no. 3, pp. 515–518, 2012.
[46] W. Saito *et al.*, "High breakdown voltage AlGaN-GaN power-HEMT design and high current density switching behavior," *IEEE Trans. Electron Devices*, vol. 50, no. 12, pp. 2528–2531, Dec. 2003.
[47] A. Lidow, M. De Rooij, J. Strydom, D. Reusch, and J. Glaser, *GaN Transistors for Efficient Power Conversion*. Hoboken, NJ, USA: Wiley, 2019.
[48] D. Zhang, Z. Yang, P. Li, M. Pang, and Q. Xue, "Flexible self-powered high-performance ammonia sensor based on Au-decorated MoSe2 nanoflowers driven by single layer MoS2-flake piezoelectric nanogenerator," *Nano Energy*, vol. 65, Nov. 2019, Art. no. 103974.
[49] X. Zhang, L. Liu, J. Wang, and Z. Wang, "Detection of SF6 decomposition components by pristine and Cr-doped GaN based on the first-principles theory," *Comput. Theor. Chem.*, vol. 1205, Nov. 2021, Art. no. 113431.
[50] W. Zhang *et al.*, "Ultrafine tungsten oxide nanowires: Synthesis and highly selective acetone sensing and mechanism analysis," *ACS Appl. Mater. Interfaces*, vol. 12, no. 3, pp. 3755–3763, 2020.
[51] M. Brandbyge, J.-L. Mozos, P. Ordejón, J. Taylor, and K. Stokbro, "Density-functional method for nonequilibrium electron transport," *Phys. Rev. B, Condens. Matter*, vol. 65, no. 16, 2002, Art. no. 165401.